Atmospheric Environment 383 (2026) 122289

Contents lists available at ScienceDirect

Atmospheric Environment

journal homepage: www.elsevier.com/locate/atmosenv

Arctic transport of North American and Canadian wildfire aerosols

Rebecca McCerery[a,*,1], Anil Namdeo[a], Lucie Malard[b], John Woodward[a], David A. Pearce[a,c]

[a] School of Geography and Natural Sciences, Northumbria University, Newcastle Upon Tyne, United Kingdom
[b] Department F.-A. Forel for Environmental and Aquatic Sciences, University of Geneva, Geneva, 1211, Switzerland
[c] British Antarctic Survey, Cambridge, United Kingdom

HIGHLIGHTS

- Shipborne PM monitoring documented four pollution events.
- Smoke and PM detected outside of wildfire smoke product ranges.
- HYSPLIT back-trajectory analysis confirmed Canadian origins for air masses.

ARTICLE INFO

Keywords:
Wildfire
Aerosols
Volatile organic compounds
$PM_{2.5}$
Air pollution
Smoke
Particulate matter
PM_{10}
Fine particulates
Coarse particulates

ABSTRACT

Wildfires are becoming increasingly frequent and intense under ongoing climate change, with the potential to emit and transport particles, from black carbon to nutrient-bearing aerosols, into remote and fragile ecosystems such as the Arctic. Yet, direct observations of long-range wildfire aerosol transport into the Arctic remain scarce, limiting our understanding of its impacts on the wider ecosystem and human health. Here, we present shipborne particulate matter (PM) measurements documenting the spatial extent and characteristics of PM in the Arctic during the 2023 North American and Canadian wildfires. Semi-continuous monitoring aboard an icebreaker from 12th September to 11th October 2023, spanning 11,000 km from Iceland to Alaska via the Northwest Passage, measured PM size fractions ($PM_{0.3}$, $PM_{0.5}$, $PM_{1.0}$, $PM_{2.5}$, PM_5 and PM_{10}) at 1-min intervals. This identified four high PM events along the cruise track, with the most intense event occurring on 28th September, when visible wildfire smoke was observed north of Victoria Island, coinciding with a peak $PM_{2.5}$ count of 58×10^6 counts m^{-3}. This smoke event was not detected by the National Oceanic and Atmospheric Administration Hazard Mapping System Fire and Smoke Product, highlighting limitations of satellite-derived smoke monitoring in remote regions. Daily mean $PM_{2.5}$ concentrations were also compared to the WHO 24-hr guidelines, where they spiked at or above the 15 $\mu g\, m^{-3}$ 24-hr guideline during the latter part of the cruise. These findings demonstrate the potentially extensive reach of North American and Canadian wildfire aerosols into the Arctic, with implications for remote community health and the adequacy of current smoke monitoring frameworks.

1. Introduction

Wildfires are becoming increasingly common with ongoing climate change (e.g., Bolan et al., 2025; Di Virgilio et al., 2019; Jones et al., 2020, 2022; Pausas and Keeley, 2021). They are unplanned, uncontrollable and unpredictable events, making them difficult to forecast, and once started can result in devastating consequences such as habitat loss, damage to infrastructure, as well as chronic health impacts and death from particulate matter (PM) (Hirsch and Koren, 2021; Mangeon et al., 2016; Roşu et al., 2025). Instances of wildfires in the United States and Canada have increased over the last two decades, and their frequency and intensity are expected to accelerate (Iglesias et al., 2022; Jones et al., 2022; Qiu et al., 2025; Wang et al., 2024).

This has serious local implications for the environment and human health, with fine particulate matter ($PM_{2.5}$) concentrations from wildfires reversing multi decadal progress in reducing concentrations from

* Corresponding author.
E-mail address: r.mccerery@northumbria.ac.uk (R. McCerery).
[1] Present Address: Department of Earth and Environmental Sciences, The University of Manchester, Manchester, United Kingdom.

https://doi.org/10.1016/j.atmosenv.2026.122289
Received 29 April 2026; Received in revised form 5 August 2026; Accepted 7 August 2026
Available online 8 August 2026

anthropogenic sources by as much as 50% in some states (Burke et al., 2023). These effects may also become far-reaching, as low-pressure systems can transport aerosols from the midlatitudes northward into the Arctic (Stohl et al., 2006; Sato et al., 2025;Yasunari et al., 2021). This has consequences for particle loading in the atmosphere and can transport black and organic carbon, impacting surface albedo on glacier and ice surfaces (Ardyna et al., 2022; Cho et al., 2025; Popovicheva et al., 2022).

Wildfire smoke reaching the Arctic can also be long-lasting. The Multidisciplinary drifting Observatory for the Study of Arctic Climate (MOSAIC) expedition onboard the Polarstern icebreaker detected a 10 km-deep aerosol layer in the upper troposphere and lower stratosphere that was present for much of the 2019/20 winter season until the collapse of the polar vortex in April 2020 (Engelmann et al., 2021; Ohneiser et al., 2021). It is thought this aerosol layer originated from wildfires in Central and Eastern Siberia from July to August 2019 and persisted for a year, trapped within the polar vortex (Engelmann et al., 2021; Ohneiser et al., 2021).

The 2023 wildfire season in Canada and North America was unprecedented in both scale and intensity (Jain et al., 2024). Approximately 15 Mha of land burned in Canada, the highest amount since records began in 1972 (Jain et al., 2024; Wang et al., 2024). During this season, over 5,000 air quality alerts were issued, nearly five times the national annual average (Flood et al., 2025; Jain et al., 2024). The effects of these wildfires extended well beyond Canada, with weather systems driving smoke southward into New York and even as far east as Europe (Chen et al., 2025a,b; Evgenieva et al., 2025; Zhang et al., 2025). In Europe, an estimated 22,400 chronic deaths were attributed to the intercontinental transport of wildfire smoke from the 2023 season, of an estimated 82,100 deaths worldwide (Zhang et al., 2025). There are therefore growing concerns that long-range transport of wildfire-sourced pollutants and particles harmful to human health results in irritation of chronic health conditions such as asthma and sudden acute deaths far beyond the local areas of the fires (Zhang et al., 2025). Direct observational datasets are critical for characterising the true spatial extent of long-range wildfire smoke transport, helping to validate and constrain atmospheric transport model outputs (Flood et al., 2025).

This paper aims to document the occurrence and characteristics of wildfire-associated aerosols from the 2023 North American and Canadian wildfires transported across the Arctic. We present direct shipborne PM measurements collected aboard *Le Commandant Charcot* during a 11,000 km transect of Arctic waters from Iceland to Alaska via the Northwest Passage, a dataset unique for this wildfire season and region. We characterise particle size distributions across the transect, identify discrete long-range transport events, and evaluate the performance of the National Oceanic and Atmospheric Administration (NOAA) Hazard Mapping System (HMS) satellite-derived smoke product against our in-field observations.

2. Methods

2.1. Cruise overview and sampling protocol

Sampling was conducted on the Ponant icebreaker vessel *Le Commandant Charcot* from 12th September 2023 – 11th October 2023 on cruises CC110923 and CC051023. The route covered a total distance of approximately 11,000 km. First, departing Reykjavik, Iceland, across the Denmark Strait to south Greenland and up the west coast towards Baffin Bay. The cruise then navigated through the historic Northwest Passage south of the Queen Elizabeth Islands and north of mainland Canada before arriving at Nome, Alaska. The cruise then continued south for a further four days before reaching Seattle, United States.

PM was measured using an air quality monitor (Model 7301-AQM1, Particles Plus, Inc., Stoughton, MA, USA) at a flow rate of 0.1 CFM (2.83 LPM) at 1-min intervals, continuously for a 12-hr period from approximate local times of 6 a.m. to 6 p.m. between 13th September and 20th September and 9:30 a.m. to 9:30 p.m. between 21st September and 11th October. The air quality monitor measured temperature, CO_2, barometric pressure (BP), $PM_{0.3}$, $PM_{0.5}$, PM_1, $PM_{2.5}$, PM_5 and PM_{10} in total counts (counts m^{-3}) and $PM_{0.5}$, PM_1, $PM_{2.5}$, PM_5 and PM_{10} mass concentrations ($\mu g\ m^{-3}$). PM fractions were acquired using a continuous laser light-scattering optical method. Equipment was placed in an accessible area on a high deck towards the bow of the ship on the port side. This area was not open to passengers, and only select personnel had access. The inlet was oriented away from the ship's primary exhaust stack (powered by liquefied natural gas and electricity) and any internal air outlets to minimise the risk of onboard contamination. Post-hoc quality control removed data collected during periods when wind direction was from the ship's stack, using meteorological data provided by Ponant with relative wind direction relative to bow (0°). The instrument placement was at approximately 330°, and ship stacks were located central and aft; therefore, counts measured when relative wind direction was 150–240° were removed. Air quality was also assessed against the World Health Organisation's 24-hr $PM_{2.5}$ guideline of 15 $\mu g\ m^{-3}$ (WHO Global Air Quality Guidelines: Particulate matter, 2021).

2.2. HYSPLIT trajectory model

Back-trajectories of air masses were calculated using the NOAA Air Resources Laboratory (ARL) Hybrid Single Particle Lagrangian Integrated Trajectory (HYSPLIT) model (Rolph et al., 2017; Stein et al., 2015) to determine the origin of air masses during discrete PM events. Trajectories were computed using the online HYSPLIT interface with Global Data Assimilation System (GDAS1, 1° resolution) meteorological reanalysis fields. Backward trajectory ensembles at 6-hr intervals for a duration of 240 h towards the position of *Le Commandant Charcot* were initialised at 500 m above ground level (AGL) to capture long-distance air parcel transport pathways above the marine boundary layer and sub-cloud layer (typically at 100-200 m). Trajectories were run for four discrete events identified in the PM time series: 14th September (Denmark Strait), 25th September (north of Baffin Island), 28th September (north of Victoria Island) and 5th October (north of Alaska). Start times were set to 1200 UTC on each respective date, corresponding to the period of peak PM concentrations observed during shipborne monitoring.

2.3. Spatial and statistical analysis

Wildfire smoke extent was mapped using the NOAA HMS Fire and Smoke Product from the NOAA Satellite Products and Services Division archive (https://satepsanone.nesdis.noaa.gov/pub/FIRE/web/HMS/). HMS smoke polygons are derived from manual analysis of visible satellite imagery from GOES, MODIS, and VIIRS satellites, with smoke density classified into three qualitative fractions representing approximate ranges of $PM_{2.5}$ concentrations of light (0–10 $\mu g\ m^{-3}$), medium (10–21 $\mu g\ m^{-3}$) and heavy (21–32 $\mu g\ m^{-3}$) (NOAA).

Spatial mapping of PM data was performed in ArcGIS Pro (version 3.3.0, Esri Inc., Redlands, CA, USA). Daily summary statistics including median, mean, maximum, minimum, and standard deviations were calculated for all PM size fractions' particle counts and mass concentrations. $PM_{2.5}$ was selected for spatial visualisation as it is the standard metric used in national and international air quality guidelines, including the WHO 24-hr guideline (WHO Global Air Quality Guidelines: Particulate matter, 2021). Daily median $PM_{2.5}$ mass concentrations and counts were visualised as proportional symbols scaled to daily median values, with symbol size and colour varying proportionally to counts and concentration.

Statistical analysis of the particulate data was performed in RStudio (R version 4.5.1). 'PM events' were identified as days in which more than 10% of observations exceeded the 99th percentile. This was repeated for each PM fraction mass concentration and count dataset.

Kruskal-Wallis tests were then performed for each event day against all other sampling days to assess statistical significance, and a pairwise Wilcoxon rank sum test with Bonferroni correction was applied to assess differences between events (magnitude of difference, degrees of freedom and statistical significance (H-, df- and p-values) are presented here; see Supplementary Material for full statistical results). Data visualisation was performed using the ggplot2 packages (Wickham, 2009).

3. Results

3.1. Spatial distribution of $PM_{2.5}$

The spatial distribution of $PM_{2.5}$ mass concentrations and counts along the cruise track are shown in Fig. 1, alongside HMS wildfire smoke density polygons for 28th September 2023. The cruise track traversed extensive areas of light and medium density smoke originating from central Canada and North America (Fig. 1a). Observations of smoke in the Arctic were first detected on 26th September and continued until 29th September (Fig. 1b). The smoke was a dark-coloured thick haze, unlike the common Arctic fog experienced throughout the rest of the cruise (Fig. 1c). However, the extent of the HMS wildfire smoke product did not extend into the cruise trajectory on the days smoke was detected (Fig. 1a). This peak in smoke observation also coincided with a spike in $PM_{2.5}$ counts on 28th of September with a maximum value of 58×10^6 counts m^{-3} and a daily mean of $11 \times 10^6 \pm 14 \times 10^6$ counts m^{-3} to the north of Victoria Island whilst navigating the remote Northwest Passage (Figs. 1a and 2a).

A time series of daily aerosol particle counts showed median values of $PM_{2.5}$ were below 1×10^7 counts m^{-3} for 24 of the 30 sampling days (Fig. 2a). There were some moderately elevated concentrations on September 15th (2×10^7 counts m^{-3}) and October 7th (1×10^7 counts m^{-3}) (Fig. 2a). The largest peak in $PM_{2.5}$ concentration occurred on 7th October (Fig. 2b), which did not coincide with the peak in $PM_{2.5}$ counts which occurred on the 28th September. $PM_{2.5}$ concentrations were also compared to the WHO guidelines (Fig. 2b). The daily mean $PM_{2.5}$ concentrations exceeded the WHO 24-hr guideline ($15\ \mu g\ m^{-3}$) on 15th September, 7th October, 10th October and 11th October during the 12-hr monitoring period. The most concerning $PM_{2.5}$ concentrations reached daily means of $40\ \mu g\ m^{-3}$, although this did not coincide with any observations of wildfire smoke. It should be noted that with this comparison, we did not monitor the full 24-hr period and therefore cannot make a direct comparison to the WHO guidelines.

3.2. Size fraction characteristics of aerosol counts and mass concentrations

Size-resolved particle counts and mass concentrations were examined across all measured size fractions from $PM_{0.3}$ to PM_{10} (Figs. 3 and 4), with discrete PM events defined as sampling days during which more than 10% of 1-min observations exceeded the 99th percentile of the full cruise distribution, calculated separately for each metric (shown in grey). This identified four PM events: (i) 14th September 2023, Denmark Strait (60.14°N, 44.28°W); (ii) 25th September 2023, Northwest Passage (77.19°N, 109.71 °W); (iii) 28th September 2023, north of Victoria Island (74.85 °N, 133.13 °W); and (iv) 7th October 2023, north of Alaska (54.29 °N, 164.67 °W).

All events showed statistically significant elevated levels of PM counts and mass concentrations (see Supplementary Materials). Event 1 on 14th September close to the Denmark Strait was characterised by statistically significant elevation in the fine particle fractions (Fig. 3). $PM_{0.3}$ counts showed the biggest difference (H = 158.7, df = 1, $p = 2.15 \times 10^{-36}$), with a median of 1.30×10^7 counts m^{-3} compared to 8.02×10^6 counts m^{-3} on all other sampling days. In contrast, $PM_{2.5}$, PM_5 and PM_{10} counts showed no statistically significant elevation on this date (all $p > 0.05$). Mass concentration data was also only significantly different in the fine fractions $PM_{0.5}$ (H = 260.8, df = 1, $p = 1.17 \times 10^{-58}$), PM_1 (H = 89.7, df = 1, $p = 2.84 \times 10^{-21}$) and $PM_{2.5}$ (H = 32.1, df = 1, $p = 1.43 \times 10^{-8}$), whilst coarse fraction concentrations (PM_5 and PM_{10}) were not significantly elevated ($p > 0.05$).

Events 2 and 3 on 25th and 28th September around the Northwest Passage were both elevated in all counts and mass concentrations (apart from PM_1 in Event 3), with Kruskal-Wallis H statistics ranging from 70.8 (PM_5 mass concentration) to 285.1 (PM_{10} counts), df = 1, $p < 0.001$. For both events, the coarse particle fractions showed substantially greater relative elevation, with PM_{10} counts an order of magnitude higher than all other sampling days (Fig. 3). Mass concentration data showed a similar pattern, with PM_5 and PM_{10} median concentrations of $223\ \mu g\ m^{-3}$ and $527\ \mu g\ m^{-3}$ respectively, compared to $18.3\ \mu g\ m^{-3}$ and $24.5\ \mu g\ m^{-3}$ across all other sampling days during Event 3 (Fig. 4). The fine fraction mass concentrations were 2–3 times higher than all other sampling days (Fig. 4).

Event 4 on 7th October north of Alaska showed a statistically significant elevation across all measured size fractions in both particle counts and mass concentrations (H ranging from 584.0 to 1063.5, df = 1, $p < 0.001$), with the largest H statistics of all four identified events. $PM_{0.3}$ counts were 3 times higher (median 2.52×10^7 counts m^{-3} vs 7.80×10^6 counts m^{-3}, H = 801.8, $p = 2.20 \times 10^{-176}$) and $PM_{2.5}$ counts 8 times higher (median 1.80×10^6 counts m^{-3} vs 2.14×10^5 counts m^{-3}, H = 994.8, $p = 2.39 \times 10^{-218}$) than all other sampling days. Mass concentration data for Event 4 showed the most pronounced elevation of all four events across all size fractions (Fig. 4). $PM_{2.5}$ mass concentrations (median $20.4\ \mu g\ m^{-3}$ vs $3.13\ \mu g\ m^{-3}$, H = 1063.5, $p = 2.79 \times 10^{-233}$) exceeded the WHO 24-hr guideline of $15\ \mu g\ m^{-3}$ during the 12-hr monitoring period.

A pairwise comparison of the four events showed differences in their PM size contribution in addition to their shared elevation above background. Events 1 and 2, and Events 3 and 4 were not significantly different in their $PM_{0.3}$ counts ($p = 1$ and $p = 0.074$ respectively). PM_{10} mass concentrations for Events 3 and 4 were also statistically indistinguishable ($p = 0.680$), whilst Event 1 showed significantly lower coarse fraction concentrations than all other events (all $p < 2 \times 10^{-14}$). For $PM_{2.5}$ counts, all event pairs were significantly different from each other except Events 3 and 4, which were statistically indistinguishable ($p = 1.000$), indicating comparable particle loads between the 28th September event in the Northwest Passage and the northern Alaska coastal event on 7th October. For $PM_{2.5}$ mass concentrations, Events 1 and 2 were not significantly different from each other ($p = 0.074$), whereas Event 4 showed the highest $PM_{2.5}$ mass concentrations of the cruise, significantly exceeding all other events (all $p < 2 \times 10^{-16}$).

3.3. Air mass back-trajectory analysis

To assess the potential origin of air masses during the identified PM events, HYSPLIT back-trajectory analyses were performed for 14th September, 25th September, 28th September and 7th October (Fig. 5). For Event 1 on 14th September in the Denmark Strait (Fig. 5a), the ensemble trajectories showed a broadly consistent origin over northern Canada with the majority of air masses tracking eastward. Air mass trajectories for Event 2 on 25th September showed a more complex and recirculating pattern, with air masses originating from northern Canada and the Canadian Arctic Archipelago before recirculating over the Arctic (Fig. 5b). Altitude profiles indicated transport largely below 1500 m AGL.

For Event 3 on 28th September north of Victoria Island (Fig. 5c), the ensemble trajectories showed the majority of air masses originated from northern and central Canada, with trajectories converging over the Canadian Arctic before arriving at the vessel position. Four trajectories (shown in green, purple, blue, yellow and red) extended significantly further west toward the North Pacific and Alaska, suggesting occasional contributions from westerly air masses, though this represents a minority of ensemble members. Altitude profiles showed a single outlier trajectory reaching approximately 5000 m AGL, indicating elevated

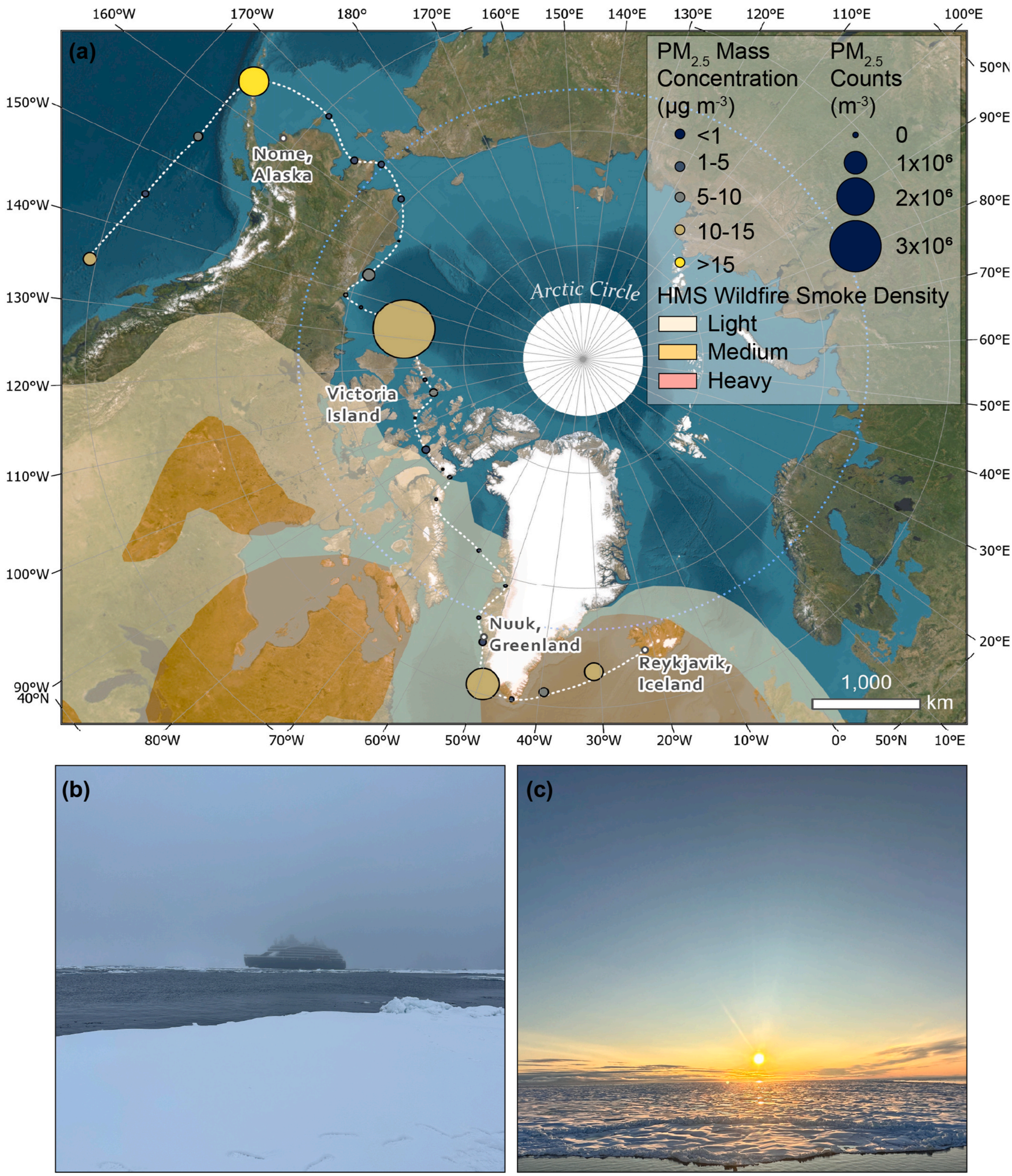

Fig. 1. (a) Spatial distribution of the aggregated daily median $PM_{2.5}$ mass concentrations (μg m^{-3}) and particle counts (counts m^{-3}) along the cruise track (white dashed line) of *Le Commandant Charcot*. Symbol colour represents daily median $PM_{2.5}$ mass concentration categorised according to WHO 24-hr guideline thresholds (WHO Global Air Quality Guidelines: Particulate matter, 2021). Symbol size represents daily median $PM_{2.5}$ particle counts (counts m^{-3}). Smoke extent mapped using the NOAA/NESDIS Hazard Mapping System (HMS) smoke product, showing light, medium, and heavy density smoke polygons for 28th September 2023 at the mid-point of the cruise when smoke was visible from the vessel. Satellite images and Arctic Circle sourced from ESRI basemap imagery | Powered by Esri. (b) 28th September 2023 at 74.84° N 133.14° W to the north of Victoria Island. (c) Comparative view on the previous smoke-free day, the 24th September 2023 at 75.10080° N, 102.81820° W. (For interpretation of the references to colour in this figure legend, the reader is referred to the Web version of this article.)

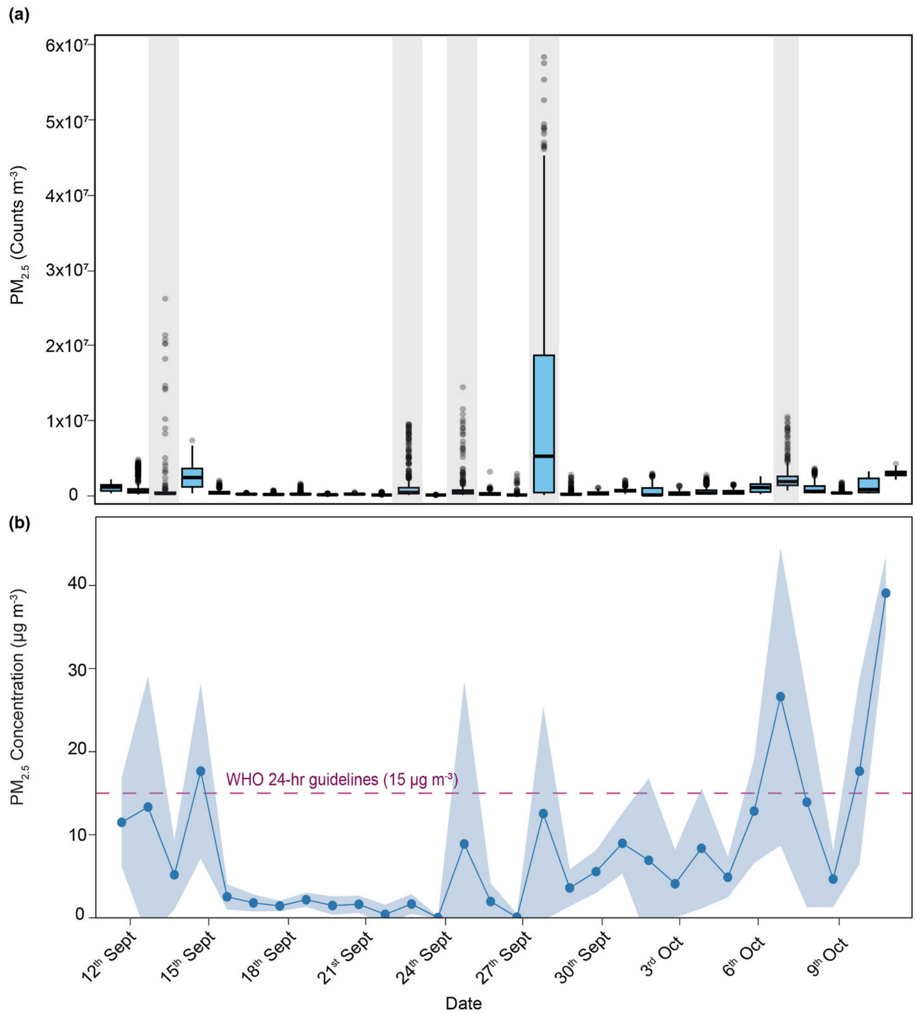

Fig. 2. (a) Time series of $PM_{2.5}$ counts over the duration of the cruise. The grey highlighted areas represent PM count events where over 10% of daily observations were above the 99th percentile. (b) Time series of $PM_{2.5}$ concentrations measured onboard *Le Commandant Charcot*, compared with 24-hr recommended limits set by the (WHO Global Air Quality Guidelines: Particulate matter, 2021)of 15 μg m^{-3} denoted by the pink dashed line. (For interpretation of the references to colour in this figure legend, the reader is referred to the Web version of this article.)

long-range transport for this ensemble member.

For Event 4 on 7th October north of Alaska (Fig. 5d), trajectories showed a different pattern from the three preceding events. Air masses originated predominantly from the North Pacific Ocean and the Bering Sea region, with several ensemble members circulating over the Aleutian Islands and the Gulf of Alaska prior to arrival at the vessel. A subset of trajectories also traced back toward Siberia and Russia. These trajectories showed substantially less spatial overlap with active Canadian wildfire regions compared to Events 1–3. Altitude profiles indicated transport predominantly below 3000 m AGL, with greater vertical variability than Events 1 and 2.

4. Discussion

4.1. Potential for long-range transport of wildfire smoke particulate matter

The data showed distinct periods of high PM counts and concentrations during the cruise trajectory in discrete events on (i) 14th September which coincided with an approach to the southern tip of Greenland, (ii) 25th September whilst passing through the Northwest Passage in proximity to an area of low smoke density from the North American and Canadian wildfires, (iii) 28th September which coincided with visible evidence of smoke from onboard *Le Commandant Charcot* and (iv) 7th October whilst traversing north of Alaska before arriving in Nome. The pairwise comparisons of these events indicated that whilst they all represented significantly elevated above background conditions, the events differed in both magnitude and size fraction characteristics. The transport pathways of air masses contributing to these PM events were also identified using HYSPLIT back-trajectory analysis, which has been applied to document long-range wildfire aerosol transport pathways across multiple regions, including Europe (e.g., Filonchyk and Peterson, 2024; Malytska and Chiriacò, 2026).

Events 1 and 2 showed $PM_{0.3}$–PM_1 fraction-dominated signals consistent with aged accumulation-mode wildfire smoke that has been transported long distances (e.g., Evgenieva et al., 2025; Filonchyk and Peterson, 2024; Kleinman et al., 2020; Lu et al., 2025). The 22nd September (three days before Event 2) also marked the largest single-day area burned in Canada since records began (440,000 ha), likely providing some of the source material for the elevated PM concentrations observed across subsequent events (Jain et al., 2024). However, long-range anthropogenic pollution cannot be entirely excluded here.

Event 3 coincided with observations of smoke from onboard *Le Commandant Charcot* and elevated total PM concentrations with a distinct coarse particle component (<10 μm, up to 5% of total). This coincided with reports of thick wildfire smoke in Nuuk, Greenland, which was covered extensively in news reports, approximately 2700 km

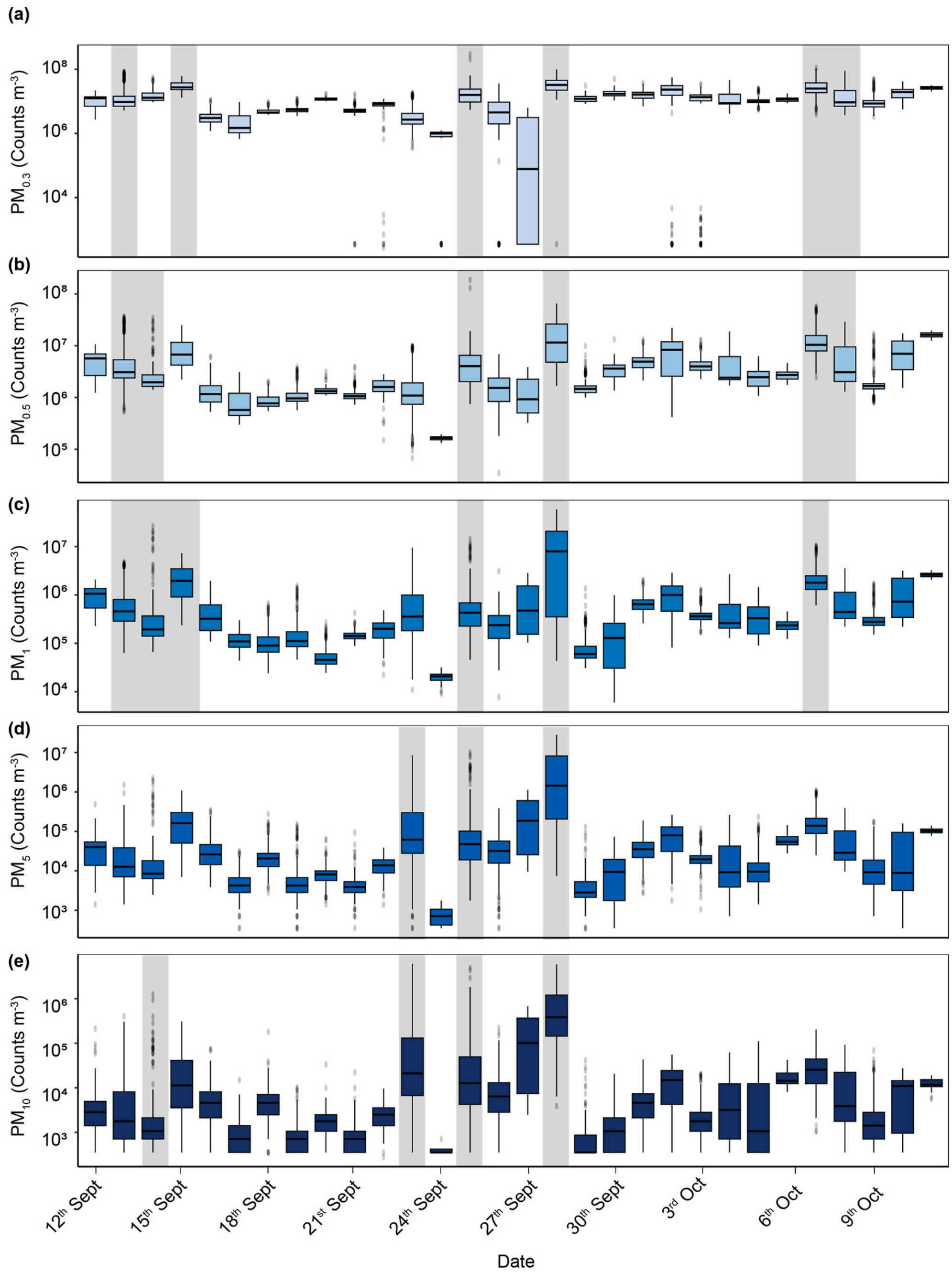

Fig. 3. Time series comparison of PM counts for fractions (a) $PM_{0.3}$, (b) $PM_{0.5}$, (c) PM_1, (d) PM_5, (e) PM_{10} over the entire study period. Box plots show the median (centre line), interquartile range (IQR, box limits), and 1.5 × IQR (whiskers). Points beyond the whiskers represent individual outliers. Highlighted regions represent days where more than 10% of counts were above the 99th percentile of the whole dataset.

east of the ship position on the same day. Reports from the Danish Meteorological Institute (DMI) and Greenland state media KNR radio mentioned the use of streetlights during the daytime due to the extent of sky darkening from the smoke, and residents reported a strong smell of smoke (Raidió Teilifís Éireann News, 2023). HYSPLIT back-trajectory ensembles also indicated air parcels originated from northern Canada in the ten days prior, coinciding with particularly high burn days in the Canadian wildfire season (Jain et al., 2024). However, the coarse fraction elevation relative to fine fractions is inconsistent with purely long-range transported aged wildfire smoke, in which coarse combustion products including ash are rapidly deposited during atmospheric transport (Kleinman et al., 2020). The coarse fraction signal is more consistent with a potential sea spray contribution (e.g., Liu et al., 2021), whilst the fine fraction elevation and visual smoke observations are consistent with long-range transported wildfire aerosol.

Event 4 showed proportionally greater elevation in coarser fractions in both counts and mass concentrations. This coincided with the proximity of the vessel to large coastal settlements near Nome, Alaska. The elevated $PM_{2.5}$ concentrations during Event 4 are less likely to be long-range wildfire transport, as HYSPLIT back-trajectory ensembles indicated air mass origins from the North Pacific and Bering Sea region rather than from active Canadian wildfire areas. During this time, no visible wildfire smoke was detected onboard, and we monitored PM for 12-hr periods as opposed to 24-hr; therefore, the WHO $PM_{2.5}$ guideline exceedances recorded during these periods are presented as contextual observations on regional air quality and are not attributed to wildfire smoke.

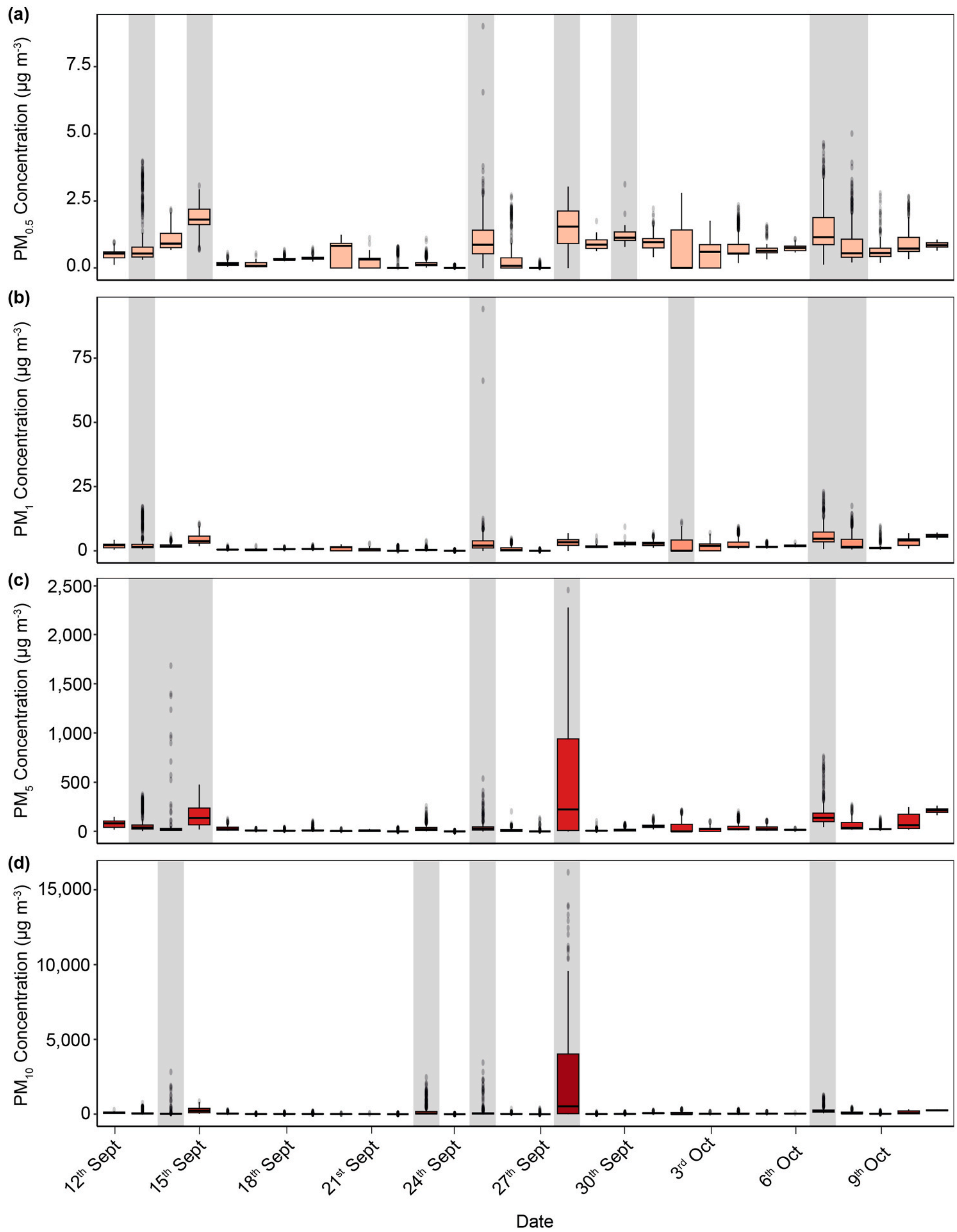

Fig. 4. Time series comparison of PM mass concentrations for fractions (a) $PM_{0.5}$, (b) PM_1, (c) PM_5, (d) PM_{10} over the entire study period. Box plots show the median (centre line), interquartile range (IQR, box limits), and 1.5 × IQR (whiskers). Points beyond the whiskers represent individual outliers. Highlighted regions represent days where more than 10% of counts were above the 99th percentile of the whole dataset.

The intercontinental transport of smoke from the 2023 Canadian fires was also documented across multiple other regions at the time. Filonchyk and Peterson (2024) recorded significantly elevated aerosol loads south of the wildfire events at El Arenosillo, Spain, attributing the signal to smoke transport from the Canadian fires. Roşu et al. (2026) also demonstrated that the 2023 Canadian fires contributed to the driest Indian monsoon August since records began in 1901. The Arctic PM observations presented here therefore represent one component of a globally significant atmospheric event affecting systems around the world.

4.2. Air quality and environmental impacts of smoke particulates

The results presented here demonstrate that potential long-range transport of PM originating from wildfires in North America and Canada reached remote parts of the Arctic. The scale of health impacts from the 2023 Canadian wildfire season was substantial. Model estimates by Zhang et al. (2025) approximate that 82,100 chronic premature deaths occurred globally in 2023 owing to smoke exposure from the Canadian wildfires, with an estimated 22,400 of these attributed to intercontinental transport reaching Europe alone. More locally, hospital admissions for asthma-related conditions peaked with a 23.6% increase in Ontario, Canada in early June, with lags in admissions estimated at 1 to 5 days post-smoke exposure (Chen et al., 2025a). The PM detected in the remote Arctic represents an extension of this same smoke transport system into one of the most sparsely monitored regions on Earth, where baseline air quality data are limited and vulnerable indigenous and remote communities have little capacity for warning or protective response. The 2023 Canadian wildfire season was further followed by continued elevated fire activity in 2024 (Filonchyk et al., 2025), suggesting that the transport pathways identified in this study are likely to recur with increasing frequency, affecting remote Arctic communities and ecosystems.

These observations highlight a critical gap in PM monitoring, which

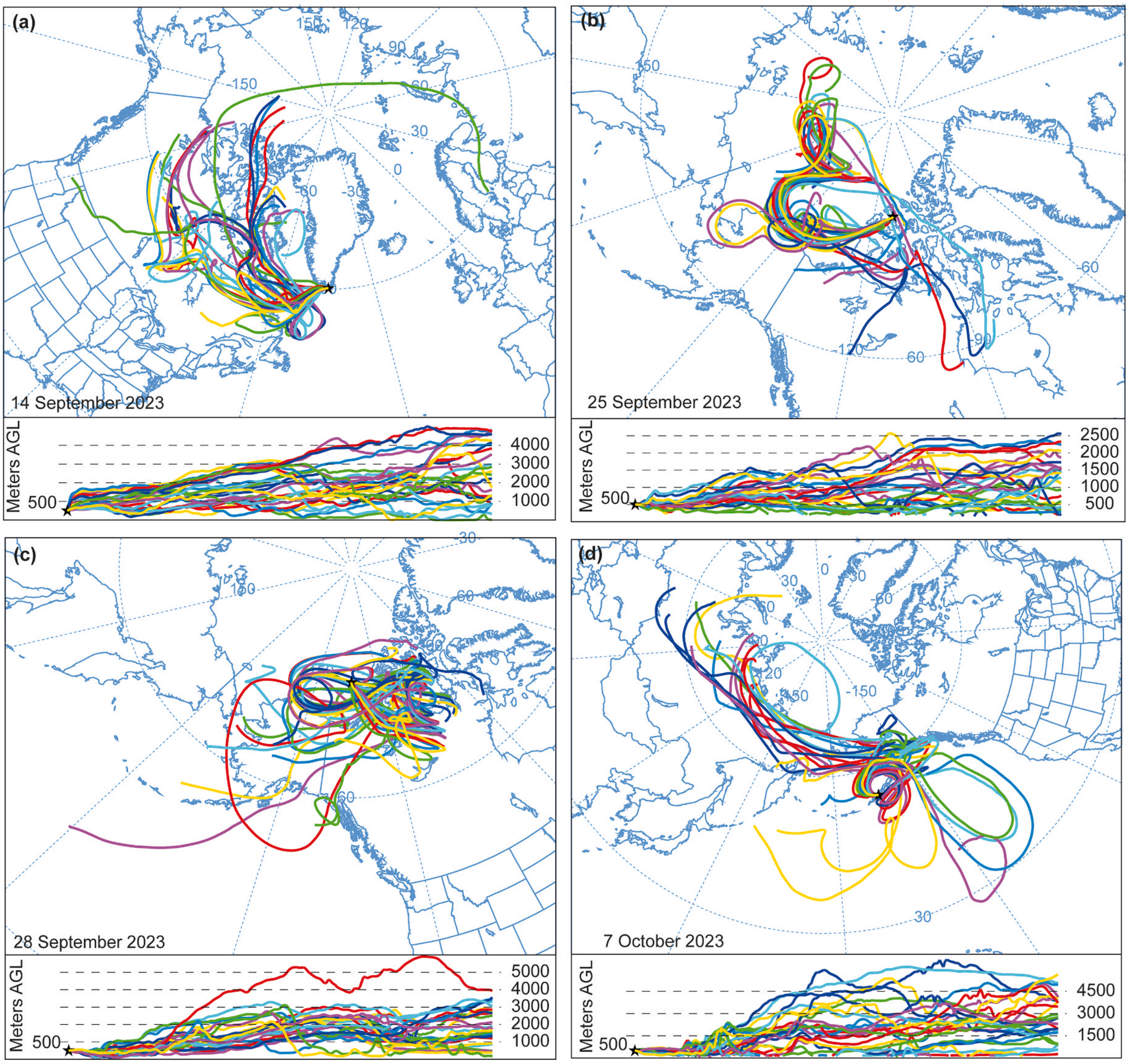

Fig. 5. NOAA HYSPLIT back-trajectory ensemble analyses for the four discrete PM events identified along the cruise track of *Le Commandant Charcot*: (a) 14th September 2023, Denmark Strait, (b) 25th September 2023, Northwest Passage, (c) 28th September 2023, north of Victoria Island and (d) 7th October 2023, north of Alaska. Each ensemble comprises multiple backward trajectories prior to the time of the PM events at each location. The lower panel shows the altitude profile of each trajectory. Trajectories were computed using the NOAA ARL HYSPLIT model (Rolph et al., 2017; Stein et al., 2015).

limits our understanding of wildfire smoke transport as well as the environmental and health impacts in remote regions. Here, we detected daily mean $PM_{2.5}$ concentrations which exceeded 15 μg m^{-3} during the latter part of the measurement period, yet the peak smoke event on 28th September was not captured by the HMS satellite-derived smoke product in this region. The HMS product was designed primarily to monitor smoke over North America and Canada, and its reduced sensitivity in remote Arctic regions represents a meaningful limitation for public health protection. Ground-level and shipborne observations such as those presented here are therefore not merely supplementary to satellite products but may be the only reliable means of detecting smoke incursion in high-latitude remote environments. This finding supports calls for expanded Arctic air quality monitoring infrastructure, including consideration of low-cost sensor networks at Arctic research stations and integration of cruise-based measurements into operational monitoring frameworks.

5. Conclusions

Here we detected wildfire particle transport across the Arctic, documenting the spatial extent and characteristics of the 2023 North American and Canadian wildfires from Iceland to Alaska. Using semi-continuous monitoring aboard *Le Commandant Charcot* cruise ship through September to October 2023, four PM events were detected on (i) 14th September at the southern tip of Greenland (ii) 25th September whilst passing through the Northwest Passage and an area of low smoke density from the North American and Canadian wildfires, (iii) 28th September which coincided with observations of smoke from onboard *Le Commandant Charcot* and (iv) 7th October whilst north of Alaska before arriving in Nome. The PM events through September coincided with long-range smoke transport modelled in the HMS wildfire product with air parcels originating around the location of active wildfires in the days leading up to the events, as confirmed by HYSPLIT back-trajectories. The peaks in PM and smoke observations, however, did not always overlay with the HMS wildfire product. This suggests that the HMS product, specifically designed to track and measure smoke in North America and Canada, may not always be effective at detecting smoke in some of the more remote but fragile regions of the world such as the Arctic. This suggests the Arctic may be overlooked in relation to both health and ecosystem impacts from wildfire smoke incursions. With ongoing climate change and predictions for wildfire intensity and frequency to increase, it is important to understand the extent of PM delivery to remote regions and its consequences on local communities and the Arctic ecosystem.

CRediT authorship contribution statement

Rebecca McCerery: Conceptualization, Data curation, Formal analysis, Investigation, Methodology, Validation, Visualization, Writing – original draft. **Anil Namdeo:** Conceptualization, Data curation, Writing – original draft. **Lucie Malard:** Conceptualization, Funding acquisition, Writing – review & editing. **John Woodward:** Funding acquisition, Resources, Writing – review & editing. **David A. Pearce:** Conceptualization, Data curation, Formal analysis, Funding acquisition, Methodology, Resources, Writing – original draft.

Declaration of competing interest

The authors declare that they have no known competing financial interests or personal relationships that could have appeared to influence the work reported in this paper.

Acknowledgements

We would like to thank PONANT EXPLORATIONS GROUP, particularly the Ponant Science Program, as well as the crew aboard *Le Commandant Charcot*, for their support during this research project. Lucie Malard was supported by the Swiss Polar Institute Exploratory Grant (SPIEG-2022-002 - ArcticAir) and the Swiss National Science Foundation (SNSF) Ambizione Fellowship (PZ00P3_223799 - Secret Invasions). The authors also gratefully acknowledge the NOAA Air Resources Laboratory (ARL) for the provision of the HYSPLIT transport and dispersion model and READY website (https://www.ready.noaa.gov) used in this publication.

Appendix A. Supplementary data

Supplementary data to this article can be found online at https://doi.org/10.1016/j.atmosenv.2026.122289.

Data availability

All data is available as Supplementary Material attached to this article.

References

Ardyna, M., Hamilton, D.S., Harmel, T., Lacour, L., Bernstein, D.N., Laliberté, J., Horvat, C., Laxenaire, R., Mills, M.M., van Dijken, G., Polyakov, I., 2022. Wildfire aerosol deposition likely amplified a summertime Arctic phytoplankton bloom. Commun. Earth Environ. 3 (1), 201. https://doi.org/10.1038/s43247-022-00511-9.

Bolan, S., Sharma, S., Mukherjee, S., Isaza, D.F.G., Rodgers, E.M., Zhou, P., Hou, D., Scordo, F., Chandra, S., Siddique, K.H., Bolan, N., 2025. Wildfires under changing climate, and their environmental and health impacts. J. Soils Sediments 25 (11), 3173–3197. https://doi.org/10.1007/s11368-025-04020-y.

Burke, M., Childs, M.L., de la Cuesta, B., Qiu, M., Li, J., Gould, C.F., Heft-Neal, S., Wara, M., 2023. The contribution of wildfire to PM2. 5 trends in the USA. Nature 622 (7984), 761–766. https://doi.org/10.1038/s41586-023-06522-6.

Chen, H., Kaufman, J.S., Chen, C., Wang, J., Maier, A., van Dijk, A., Slipp, N., Rana, J., MacIntyre, E., Su, Y., Kim, J., 2025b. Impact of the 2023 wildfire smoke episodes in Ontario, Canada, on asthma and other health outcomes: an interrupted time-series analysis. CMAJ (Can. Med. Assoc. J.) 197 (17), E465–E477. https://doi.org/10.1503/cmaj.241506.

Chen, H., Zhang, W., Sheng, L., 2025a. Canadian record-breaking wildfires in 2023 and their impact on US air quality. Atmos. Environ. 342, 120941. https://doi.org/10.1016/j.atmosenv.2024.120941.

Cho, Y., Kim, H., Park, R.J., Kim, S.W., 2025. Unprecedented east Siberian wildfires intensify Arctic snow darkening through enhanced poleward transport of black carbon. Sci. Total Environ. 961, 178423. https://doi.org/10.1016/j.scitotenv.2025.178423.

Di Virgilio, G., Evans, J.P., Blake, S.A., Armstrong, M., Dowdy, A.J., Sharples, J., McRae, R., 2019. Climate change increases the potential for extreme wildfires. Geophys. Res. Lett. 46 (14), 8517–8526. https://doi.org/10.1029/2019GL083699.

Engelmann, R., Ansmann, A., Ohneiser, K., Griesche, H., Radenz, M., Hofer, J., Althausen, D., Dahlke, S., Maturilli, M., Veselovskii, I., Jimenez, C., 2021. Wildfire smoke, Arctic haze, and aerosol effects on mixed-phase and cirrus clouds over the North Pole region during MOSAiC: an introduction. Atmos. Chem. Phys. 21 (17), 13397–13423. https://doi.org/10.5194/acp-21-13397-2021.

Evgenieva, T., Dosev, S., Gurdev, L., Vulkova, L., Peshev, Z., Toncheva, E., Popov, L., Vankov, O., Dreischuh, T., 2025. Canadian wildfire smoke episode over Europe in October 2023: Lidar, sun-photometer, and model characterization of smoke layers observed above Sofia, Bulgaria. Remote Sens. 17 (16), 2899. https://doi.org/10.3390/rs17162899.

Filonchyk, M., Peterson, M.P., 2024. Changes in aerosol properties at the El Arenosillo site in Southern Europe as a result of the 2023 Canadian forest fires. Environ. Res. 260, 119629. https://doi.org/10.1016/j.envres.2024.119629.

Filonchyk, Mikalai, Peterson, Michael P., Zhang, Liming, Zhang, Lifeng, He, Yi, 2025. Estimating air pollutant emissions from the 2024 wildfires in Canada and the impact on air quality. Gondwana Research 140, 194–204. https://doi.org/10.1016/j.gr.2024.12.012. https://linkinghub.elsevier.com/retrieve/pii/S1342937X25000152.

Flood, V.A., Strong, K., Whaley, C.H., Chen, J., Wunch, D., Drummond, J.R., Colebatch, O., Gillespie, L., Mostafavi Pak, N., 2025. The impact of the 2023 Canadian forest fires on air quality in southern Ontario. J. Geophys. Res. Atmos. 130 (5), e2024JD042254. https://doi.org/10.1029/2024JD042254.

Hirsch, E., Koren, I., 2021. Record-breaking aerosol levels explained by smoke injection into the stratosphere. Science 371 (6535), 1269–1274. https://doi.org/10.1126/science.abe1415.

Iglesias, Virginia, Stavros, Natasha, Balch, Jennifer K, Barrett, Kimiko, Cobian-Iñiguez, Jeanette, Hester, Cyrus, Kolden, Crystal A, Leyk, Stefan, Nagy, R Chelsea, Reid, Colleen E, Wiedinmyer, Christine, Woolner, Elizabeth, Travis, William R, 2022. Fires that matter: reconceptualizing fire risk to include interactions between humans and the natural environment. Environmental Research Letters 17 (4), 045014. https://doi.org/10.1088/1748-9326/ac5c0c. https://iopscience.iop.org/article/10.1088/1748-9326/ac5c0c. (Accessed 24 March 2022).

Jain, P., Barber, Q.E., Taylor, S.W., Whitman, E., Castellanos Acuna, D., Boulanger, Y., Chavardès, R.D., Chen, J., Englefield, P., Flannigan, M., Girardin, M.P., 2024. Drivers and impacts of the record-breaking 2023 wildfire season in Canada. Nat. Commun. 15 (1), 6764. https://doi.org/10.1038/s41467-024-51154-7.

Jones, M.W., Abatzoglou, J.T., Veraverbeke, S., Andela, N., Lasslop, G., Forkel, M., Smith, A.J., Burton, C., Betts, R.A., van der Werf, G.R., Sitch, S., 2022. Global and regional trends and drivers of fire under climate change. Rev. Geophys. 60 (3), e2020RG000726. https://doi.org/10.1029/2020RG000726.

Jones, M.W., Smith, A., Betts, R., Canadell, J.G., Prentice, I.C., Le Quéré, C., 2020. Climate Change Increases the Risk of Wildfires.

Kleinman, L.I., Sedlacek III, A.J., Adachi, K., Buseck, P.R., Collier, S., Dubey, M.K., Hodshire, A.L., Lewis, E., Onasch, T.B., Pierce, J.R., Shilling, J., 2020. Rapid evolution of aerosol particles and their optical properties downwind of wildfires in the western US. Atmos. Chem. Phys. 20 (21), 13319–13341. https://doi.org/10.5194/acp-20-13319-2020.

Liu, S., Liu, C.C., Froyd, K.D., Schill, G.P., Murphy, D.M., Bui, T.P., Dean-Day, J.M., Weinzierl, B., Dollner, M., Diskin, G.S., Chen, G., 2021. Sea spray aerosol concentration modulated by sea surface temperature. Proc. Natl. Acad. Sci. 118 (9), e2020583118. https://doi.org/10.1073/pnas.2020583118, 2021.

Lu, S., Bhattarai, C., Samburova, V., Khlystov, A., 2025. Particle size distributions of wildfire aerosols in the Western USA. Environ. Sci. J. Integr. Environ. Res.: Atmosphere 5 (4), 502–516. https://doi.org/10.1039/D5EA00007F.

Malytska, L., Chiriacò, M.V., 2026. Where do wildfire-related emissions travel? Transport trajectories of Black carbon, organic carbon, and PM2. 5 from Italian forest fires (2008–2024). Atmos. Environ., 121922 https://doi.org/10.1016/j.atmosenv.2026.121922.

Mangeon, S., Voulgarakis, A., Gilham, R., Harper, A., Sitch, S., Folberth, G., 2016. INFERNO: a fire and emissions scheme for the UK Met Office's unified model. Geosci. Model Dev. 9 (8), 2685–2700. https://doi.org/10.5194/gmd-9-2685-2016.

NOAA. NESDIS hazard mapping system (HMS) fire and smoke product. https://satepsanone.nesdis.noaa.gov/pub/FIRE/web/HMS/.

Ohneiser, K., Ansmann, A., Chudnovsky, A., Engelmann, R., Ritter, C., Veselovskii, I., Baars, H., Gebauer, H., Griesche, H., Radenz, M., Hofer, J., 2021. The unexpected smoke layer in the high arctic winter stratosphere during MOSAiC 2019–2020. Atmos. Chem. Phys. 21 (20), 15783–15808. https://doi.org/10.5194/acp-21-15783-2021.

Pausas, J.G., Keeley, J.E., 2021. Wildfires and global change. Front. Ecol. Environ. 19 (7), 387–395. https://doi.org/10.1002/fee.2359.

Popovicheva, O.B., Evangeliou, N., Kobelev, V.O., Chichaeva, M.A., Eleftheriadis, K., Gregorič, A., Kasimov, N.S., 2022. Siberian Arctic Black carbon: gas flaring and wildfire impact. Atmos. Chem. Phys. 22 (9), 5983–6000. https://doi.org/10.5194/acp-22-5983-2022.

Qiu, M., Li, J., Gould, C.F., Jing, R., Kelp, M., Childs, M.L., Wen, J., Xie, Y., Lin, M., Kiang, M.V., Heft-Neal, S., 2025. Wildfire smoke exposure and mortality burden in the US under climate change. Nature 1–3. https://doi.org/10.1038/s41586-025-09611-w.

Raidió Teilifís Éireann, 2023. 'canadian wildfire smoke darkens Greenland skies'Raidió Teilifís Éireann, 27th September 2023, available at: https://www.rte.ie/news/world/2023/0927/1407663-greenland-canada/. (Accessed 27 November 2025).

Rolph, G., Stein, A., Stunder, B., 2017. Real-time environmental applications and display system: READY. Environ. Model. Software 95, 210–228. https://doi.org/10.1016/j.envsoft.2017.06.025.

Roşu, I.A., Mourgela, R.N., Kasoar, M., Boleti, E., Parrington, M., Voulgarakis, A., 2025. Large-scale impacts of the 2023 Canadian wildfires on the Northern hemisphere atmosphere. npj Clean Air 1 (1), 22. https://doi.org/10.1038/s44407-025-00022-9.

Roşu, I.A., Mourgela, R.N., Kasoar, M., Petrakis, M.P., Voulgarakis, A., 2026. Severe rapid Indian monsoon weakening due to emissions from extreme Canadian wildfires. npj Natural Hazards 3 (1), 19. https://doi.org/10.1038/s44304-026-00184-w.

Sato, Kazutoshi, Takahashi, Kazu, Inoue, Jun, 2025. Impact of Canadian wildfires on aerosol and ice clouds in the early-autumn Arctic. Atmospheric Research 315, 107893. https://doi.org/10.1016/j.atmosres.2024.107893, 107893. https://linkinghub.elsevier.com/retrieve/pii/S0169809524006756.

Stein, A.F., Draxler, R.R., Rolph, G.D., Stunder, B.J., Cohen, M.D., Ngan, F., 2015. NOAA's HYSPLIT atmospheric transport and dispersion modeling system. Bull. Am. Meteorol. Soc. 96 (12), 2059–2077. https://doi.org/10.1175/BAMS-D-14-00110.1.

Stohl, A., Andrews, E., Burkhart, J.F., Forster, C., Herber, A., Hoch, S.W., Kowal, D., Lunder, C., Mefford, T., Ogren, J.A., Sharma, S., 2006. Pan-Arctic enhancements of light absorbing aerosol concentrations due to North American boreal forest fires during summer 2004. J. Geophys. Res. Atmos. 111 (D22). https://doi.org/10.1029/2006JD007216.

Wang, Z., Wang, Z., Zou, Z., Chen, X., Wu, H., Wang, W., Su, H., Li, F., Xu, W., Liu, Z., Zhu, J., 2024. Severe Global Environmental Issues Caused by Canada's record-breaking Wildfires in 2023. https://doi.org/10.1007/s00376-023-3241-0.

WHO Global Air Quality Guidelines: Particulate matter, 2021. PM2.5 and PM10), Ozone, Nitrogen Dioxide, Sulfur Dioxide and Carbon Monoxide. World Health Organization, Geneva. Available at: https://www.who.int/publications/i/item/9789240034228.

Wickham, Hadley, 2009. ggplot2. Springer New York, New York, NY, ISBN 9780387981406. https://doi.org/10.1007/978-0-387-98141-3. https://link.springer.com/10.1007/978-0-387-98141-3.

Yasunari, T.J., Nakamura, H., Kim, K.M., Choi, N., Lee, M.I., Tachibana, Y., da Silva, A. M., 2021. Relationship between circum-Arctic atmospheric wave patterns and large-scale wildfires in boreal summer. Environ. Res. Lett. 16 (6), 064009. https://doi.org/10.1088/1748-9326/abf7ef.

Zhang, Q., Wang, Y., Xiao, Q., Geng, G., Davis, S.J., Liu, X., Yang, J., Liu, J., Huang, W., He, C., Luo, B., 2025. Long-range PM2. 5 pollution and health impacts from the 2023 Canadian wildfires. Nature 1–7. https://doi.org/10.1038/s41586-025-09482-1.